Terahertz holography for imaging amplitude and phase objects

Erwin Hack* **and Peter Zolliker**

Empa, Swiss Federal Laboratories for Materials Science and Technology, Laboratory for Reliability Science and Technology, 129 Uberlandstrasse, CH-8600 Dubendorf, Switzerland
**erwin.hack@empa.ch*

Abstract: A non-monochromatic THz Quantum Cascade Laser and an uncooled micro-bolometer array detector with VGA resolution are used in a beam-splitter free holographic set-up to measure amplitude and phase objects in transmission. Phase maps of the diffraction pattern are retrieved using the Fourier transform carrier fringe method; while a Fresnel-Kirchhoff back propagation algorithm is used to reconstruct the complex object image. A lateral resolution of 280 µm and a relative phase sensitivity of about 0.5 rad are estimated from reconstructed images of a metallic Siemens star and a polypropylene test structure, respectively. Simulations corroborate the experimental results.

©2014 Optical Society of America

OCIS codes: (110.6795) Terahertz imaging; (090.1995) Digital holography; (040.2235) Far infrared or terahertz; (350.5730) Resolution.

References and links

1. M. S. Vitiello, L. Consolino, S. Bartalini, A. Taschin, A. Tredicucci, M. Inguscio, and P. De Natale, "Quantum-limited frequency fluctuations in a terahertz laser," Nat. Photonics **6**(8), 525–528 (2012).
2. S. Chakraborty, O. Marshall, C. W. Hsin, M. Khairuzzaman, H. Beere, and D. Ritchie, "Discrete mode tuning in terahertz quantum cascade lasers," Opt. Express **20**(26), B306–B314 (2012).
3. J. Faist, G. Scalari, M. Fischer, and M. Beck, "Terahertz quantum cascade lasers: 10 years of active region and material progresses," 2011 36th International Conference on Infrared, Millimeter, and Terahertz Waves (Irmmw-Thz) (2011).
4. K. E. Peiponen, J. A. Zeitler, and M. Kuwata-Gonokami, *Terahertz Spectroscopy and Imaging* (Springer, Heidelberg, 2013).
5. S. H. Ding, Q. Li, R. Yao, and Q. Wang, "High-resolution terahertz reflective imaging and image restoration," Appl. Opt. **49**(36), 6834–6839 (2010).
6. P. Dean, A. Valavanis, J. Keeley, K. Bertling, Y. L. Lim, R. Alhathlool, S. Chowdhury, T. Taimre, L. H. H. Li, D. Indjin, S. J. Wilson, A. D. Rakic, E. H. Linfield, and A. G. Davies, "Coherent three-dimensional terahertz imaging through self-mixing in a quantum cascade laser," Appl. Phys. Lett. **103**(18), 181112 (2013).
7. A. D. Rakić, T. Taimre, K. Bertling, Y. L. Lim, P. Dean, D. Indjin, Z. Ikonić, P. Harrison, A. Valavanis, S. P. Khanna, M. Lachab, S. J. Wilson, E. H. Linfield, and A. G. Davies, "Swept-frequency feedback interferometry using terahertz frequency QCLs: a method for imaging and materials analysis," Opt. Express **21**(19), 22194–22205 (2013).
8. X. Gao, C. Li, and G. Y. Fang, "Study of image reconstruction for terahertz indirect holography with quasi-optics receiver," J. Opt. Soc. Am. A **30**(6), 1291–1296 (2013).
9. M. Suga, Y. Sasaki, T. Sasahara, T. Yuasa, and C. Otani, "THz phase-contrast computed tomography based on Mach-Zehnder interferometer using continuous wave source: proof of the concept," Opt. Express **21**(21), 25389–25402 (2013).
10. J. P. Guillet, B. Recur, L. Frederique, B. Bousquet, L. Canioni, I. Manek-Honninger, P. Desbarats, and P. Mounaix, "Review of Terahertz Tomography Techniques," J Infrared Millim Te **35**(4), 382–411 (2014).
11. J. F. Federici, D. Gary, B. Schulkin, F. Huang, H. Altan, R. Barat, and D. Zimdars, "Terahertz imaging using an interferometric array," Appl. Phys. Lett. **83**(12), 2477–2479 (2003).
12. X. K. Wang, Y. Cui, W. F. Sun, and Y. Zhang, ""Terahertz Digital Holography," Photonics and Optoelectronics Meetings (Poem) 2011," Laser and Terahertz Science and Technology **8330**, 833003 (2012).
13. M. Lowe, *Imaging of 3.4 THz Quantum Cascade Laser Beam Using an Uncooled Microbolometer Camera* (Monterey, 2006).
14. F. Simoens and J. Meilhan, "Terahertz real-time imaging uncooled array based on antenna- and cavity-coupled bolometers," Philos Trans A Math Phys Eng Sci **372**(2012), 20130111 (2014).

#209610 - $15.00 USD Received 7 Apr 2014; revised 23 May 2014; accepted 18 Jun 2014; published 23 Jun 2014
(C) 2014 OSA

15. B. N. Behnken, G. Karunasiri, D. R. Chamberlin, P. R. Robrish, and J. Faist, "Real-time imaging using a 2.8 THz quantum cascade laser and uncooled infrared microbolometer camera," Opt. Lett. **33**(5), 440–442 (2008).
16. K. Xue, Q. Li, Y. D. Li, and Q. Wang, "Continuous-wave terahertz in-line digital holography," Opt. Lett. **37**(15), 3228–3230 (2012).
17. N. V. Petrov, A. N. Galiaskarov, T. Y. Nikolaeva, and V. G. Bespalov, "The features of optimization of a phase retrieval technique in THz frequency range," in *Speckle 2012: V International Conference on Speckle Metrology*, (SPIE, 2012)
18. Y. Sasaki, C. Otani, H. Kasuga, H. Ohmori, M. Suga, and T. Yuasa, "Terahertz 3D imaging with a CW source and phase-shifting interferometry," in *Terahertz Physics, Devices, and Systems Vii: Advanced Applications in Industry and Defense*, (SPIE, 2013)
19. W. F. Sun, X. K. Wang, and Y. Zhang, "Continuous wave terahertz phase imaging with three-step phase-shifting," Optik (Stuttg.) **124**(22), 5533–5536 (2013).
20. S. H. Ding, Q. Li, Y. D. Li, and Q. Wang, "Continuous-wave terahertz digital holography by use of a pyroelectric array camera," Opt. Lett. **36**(11), 1993–1995 (2011).
21. Q. Li, S. H. Ding, Y. D. Li, K. Xue, and Q. Wang, "Experimental research on resolution improvement in CW THz digital holography," Appl. Phys. B **107**(1), 103–110 (2012).
22. M. Takeda, H. Ina, and S. Kobayashi, "Fourier-Transform Method of Fringe-Pattern Analysis for Computer-Based Topography and Interferometry," J. Opt. Soc. Am. **72**(1), 156–160 (1982).
23. L. Y. Qian, B. Sheng, Y. S. Huang, J. Z. Ling, R. J. Hong, D. W. Zhang, B. L. Xu, B. C. Li, Z. J. Ni, and S. L. Zhuang, "Tilted and axis-shift Lloyd's mirror system for recording low-density and large-area holographic grating," Optik (Stuttg.) **125**(3), 1287–1291 (2014).
24. V. Chhaniwal, A. S. G. Singh, R. A. Leitgeb, B. Javidi, and A. Anand, "Quantitative phase-contrast imaging with compact digital holographic microscope employing Lloyd's mirror," Opt. Lett. **37**(24), 5127–5129 (2012).
25. J. W. Goodman, *Introduction to Fourier Optics,* 2nd ed., McGraw-Hill series in electrical and computer engineering (McGraw-Hill, 1996), pp. xviii, 441 p.
26. P. Picart and J. Leval, "General theoretical formulation of image formation in digital Fresnel holography," J. Opt. Soc. Am. A **25**(7), 1744–1761 (2008).
27. G. D. Boreman, *Modulation Transfer Function in Optical and Electro-optical Systems* (SPIE Press, Bellingham, Wash., 2001).
28. M. S. Heimbeck, M. K. Kim, D. A. Gregory, and H. O. Everitt, "Terahertz digital holography using angular spectrum and dual wavelength reconstruction methods," Opt. Express **19**(10), 9192–9200 (2011).
29. H. C. Ryu, N. Kim, S. P. Han, H. Ko, J. W. Park, K. Moon, and K. H. Park, "Simple and cost-effective thickness measurement terahertz system based on a compact 1.55 μm λ/4 phase-shifted dual-mode laser," Opt. Express **20**(23), 25990–25999 (2012).
30. M. Schwerdtfeger, S. Lippert, M. Koch, A. Berg, S. Katletz, and K. Wiesauer, "Terahertz time-domain spectroscopy for monitoring the curing of dental composites," Biomed. Opt. Express **3**(11), 2842–2850 (2012).

1. Introduction

Quantum Cascade Lasers (QCL) in the THz regime provide sources of reasonable power and coherence on a small footprint to be used in interferometric experiments [1–3]. Imaging technologies based on THz coherent radiation are becoming a powerful tool for material science and mechanical engineering [4]. Scanning the object through a focused THz beam is still a popular way for obtaining images [5–7], especially for sources based on optical antennae. Alternatively, the focused beam may be scanned across the object, or a point detector is scanned across an object beam [8]. Experiments are often designed in analogy to optical techniques, such as imaging in transmission and reflection, interferometry in Mach-Zehnder [9] arrangements for digital holography or optical tomography [10].

Digital holography is of special interest if resolution has to be pushed below the diffraction limit for small objects. A precursor to digital holography with direct THz imaging was realized by Federici et al. [11] a decade ago by using a number of single detector elements from which the original field distribution from the target was reconstructed. Recently, Wang has reported a digital Terahertz holographic system [12] based on transforming the pulsed THz signal by optical rectification in a birefringent ZnTe crystal. Interferometric images were obtained when passing the THz wave through the non-linear crystal and probing the induced birefringence with an optical beam which then is used in a classical interferometer. The authors report reconstructed intensity images but no phase-maps of the object.

Different area detectors are available for direct imaging of THz radiation. Micro-bolometer arrays of 160 × 120 to 384 × 288 pixels have been shown to work with THz

#209610 - $15.00 USD Received 7 Apr 2014; revised 23 May 2014; accepted 18 Jun 2014; published 23 Jun 2014
(C) 2014 OSA

radiation [13–15]. A Pyrocam array detector with 124x124 pixels on a 100 μm pitch was reported to perform in-line holographic measurements at 2.52 THz without optical rectification [16]. The set-up was based on a collimated incoming beam, and image reconstruction was made under the assumption that the amplitude of the diffracted beam was much smaller than that of the reference beam. The reconstructed images suffer from edge diffraction artefacts. Although iterative algorithms can be used to obtain a phase distribution from intensity distributions in an in-line holographic set-up [17], a direct measurement of the phase distribution holds great promise to increase the resolution and accuracy of the holographic reconstruction. Phase shifting THz interferometry with a CW source was reported at wavelengths below 0.7 THz so far [18, 19], and that work was based on a single point detection set-up, while imaging was achieved by sample rastering. Off-axis holography using a beam splitter, a Pyrocam array detector of 124x124 pixels and Fourier retrieval of the phase distribution was reported by Ding et al. [20] for metallic objects; the lateral resolution was estimated to be better than 0.4 mm for an object size of 8 mm. Li et al. [21] assessed the resolution by improved zero-order diffraction suppression and higher numerical aperture (NA), viz. smaller recording distance. However, the pixel size of 100 μm limited the useful range of off-axis angle, and Laplacian differential reconstruction was needed to separate the overlapping zero and first-order peaks in Fourier domain. A minimum resolution of 0.17 mm was estimated from the cut-off frequency, while experimental tests based on a 10 mm diameter Siemens star yielded a resolution of 0.28 mm.

In contrast to those papers, we present a digital THz holography set-up that (i) uses a QCL at 3 THz; (ii) needs a single mirror, i.e. is free of a beam-splitter element; (iii) uses a high-resolution 480x640 pixel, uncooled micro-bolometer array with 25 μm pitch for recording the holograms; and is (iv) capable of measuring both the amplitude of a diffracted object wave as well as the phase through the Fourier method introduced in holography by Takeda et al. [22]. With our equipment, off-axis configurations can be implemented at larger angles, as the THz wavelength of around 100 μm is four times the pixel size of the detector. The proposed setup aims at applying THz holography with relatively low cost and easy-to-use equipment for the feature analysis in objects in the millimeter and centimeter range. Potential applications range from non-destructive testing of plastics, composites, electronic devices to the investigation organic material.

2. Experimental

We use a THz Quantum Cascade Laser (QCL) emitting around 3 THz (Alpes Lasers, Neuchâtel, Switzerland) with 1.2 mW peak power and 5% duty cycle cooled with liquid nitrogen. The laser emits on a few narrow wavelengths in the range from 95 to 108 μm with dominant peaks at 99.0 μm, 100.0 μm and 102.5 μm. The detector is an uncooled Vanadium Oxide micro-bolometer array (DelMar Photonics, San Diego, USA) with 640x480 pixels on a pitch of 25 μm. Images are recorded through a CameraLink interface. To eliminate the thermal background, frames with laser off are subtracted from frames with laser on using a LabView program. For increasing the signal-to-noise ratio, some 1000 frames were averaged leading to a fringe modulation of up to 7 bit.

The QCL emits a cone beam with an approximate 60° full angle which allows us to use an off-axis digital holography set-up without beam-splitter, see Fig. 1, like a Lloyd's mirror interferometer which is used in optics [23, 24] or x-ray lithography, but – to our knowledge – has not been reported for Terahertz holography so far. Part of the beam is reflected from a metallic mirror and serves as reference beam, while the direct cone beam illuminates the object, and the diffracted beam represents the object beam. This off-axis holographic set-up generates a fringe spacing of around 6 pixels (Fig. 2), i.e. 7 line pairs per mm (LP/mm), which corresponds to an interference angle of around 40°. The visibility of the fringes in this image vanishes for regions where the contributions of the different wavelengths cancel out.

#209610 - $15.00 USD Received 7 Apr 2014; revised 23 May 2014; accepted 18 Jun 2014; published 23 Jun 2014
(C) 2014 OSA

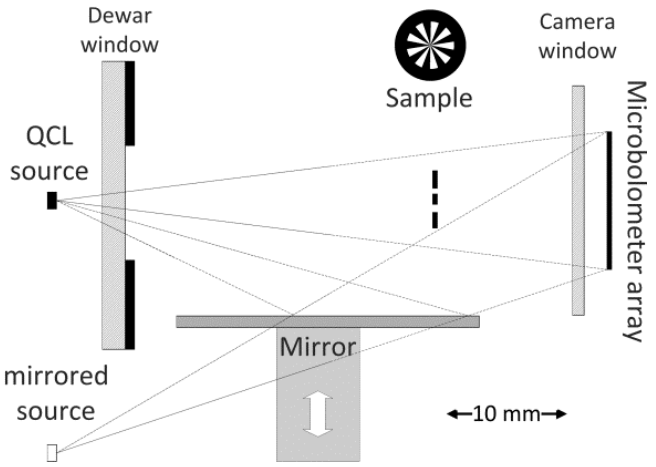

Fig. 1. Experimental set-up, schematic.

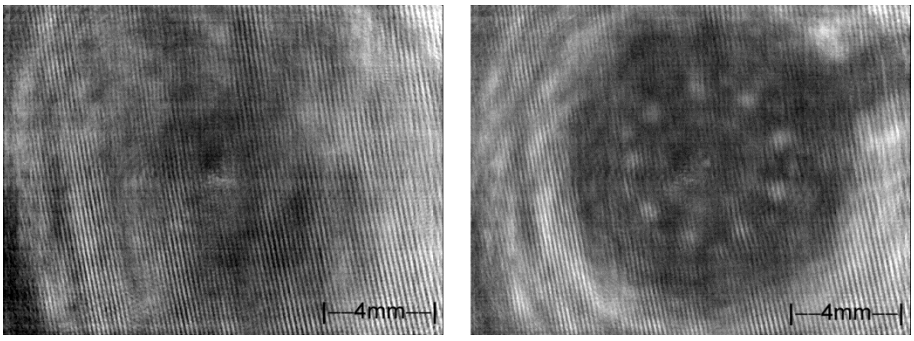

Fig. 2. Carrier fringes (left) and diffraction pattern of an object wave superposed to the reference wave (right).

After subtraction of the background the interferometric signal recorded by the bolometer is

$$I = I_{ref} + I_{obj} + 2\sqrt{I_{ref} I_{obj}} \cos\left(\varphi_{ref} - \varphi_{obj} + \delta\varphi \right), \tag{1}$$

where subscripts *ref* and *obj* refer to the reference beam and the object beam, respectively. φ is the respective phase of the waves, while $\delta\varphi$ denotes a phase step controlled by mirror translation. In order to reconstruct the object, knowledge of the amplitude and the phase of the object wave is a prerequisite. While its amplitude is readily available from the diffraction pattern (taking the square root of the intensity of the object wave measured without reference beam), the phase of the object wave is retrieved applying the Fourier transform method to the carrier frequency frames. In order to reduce systematic errors we use differences of the phases derived from measurements with and without object. Furthermore, to cope with beat frequencies from the non-monochromatic source, the quality of the phase map was improved by tiling areas with the most reliable signals from phase maps taken at different mirror positions.

3. Simulation and data evaluation

3.1 Forward and backward propagation

The diffraction pattern of the object at the detector plane is simulated by propagating the field distribution at the object plane (numerical mask) to the detector (image plane) using the

#209610 - $15.00 USD Received 7 Apr 2014; revised 23 May 2014; accepted 18 Jun 2014; published 23 Jun 2014
(C) 2014 OSA

convolution method based on the Fresnel-Kirchhoff integral [25]. We use a spherical Gaussian beam and superpose diffraction patterns from the three main emission wavelengths at 99.0, 100.0 and 102.5 μm with respective weights of 0.25, 0.25 and 0.5 corresponding to their relative strengths taken from a measured emission spectrum of the QCL. Then, the field at the image plane is sampled with the pixel resolution and size of the detector. The reconstructed complex field at the object plane is obtained using the inverse Fresnel-Kirchhoff diffraction formula. For a metallic object, the reconstructed amplitude yields the object contour with random phase at opaque areas, while for a phase object the phase distribution of the original object is obtained at the appropriate reconstruction distance.

3.2 Estimation of resolution

The reconstructed field A_R can be written as the convolution of the original object wave A with the pixel function Π_p and intrinsic resolution function W [26].

$$A_R(X,Y) = \kappa \times A(X,Y) * \prod_p (X,Y) * W(X,Y) \tag{2}$$

where κ is a complex constant. For an $N \times M$ pixel array, the functions are

$$\begin{aligned} \prod_p (X,Y) &= \begin{cases} \frac{1}{p^2} & if \quad -\frac{p}{2} \le X,Y \le \frac{p}{2} \\ 0 & otherwise \end{cases} \\ W(X,Y) &= \frac{\sin(N\xi)}{\sin(\xi)} \frac{\sin(M\eta)}{\sin(\eta)} \\ (\xi,\eta) &= \frac{\pi p}{\lambda g} \times (X,Y) \end{aligned} \tag{3}$$

where g is the reconstruction distance, λ the wavelength, and p the pitch of the square pixels. For large N, the intrinsic resolution function W is a sinc-function with a resolution d_W in X-direction estimated by the first zero occurring at $N\xi = \pi$, which is

$$d_W = \lambda \frac{g}{N p} \tag{4}$$

and correspondingly for Y. Loosely speaking, the intrinsic spatial resolution in the reconstructed field is limited by the numerical aperture of the system and the wavelength. It dominates the resolution implied by the pixel function for distances larger than

$$g \ge N \frac{p^2}{\lambda} \tag{5}$$

In our experiment the bolometer array has p = 25 μm, N = 480, while λ = 100 μm. Thus, for object distances $g \ge 3$ mm the intrinsic resolution function dominates.

The spectral spread s of the THz source also limits the obtainable resolution. An upper limit to its contribution is estimated assuming a source with two equally strong emission lines at λ_0 $(1 \pm s)$. Back propagation to a distance g using the average wavelength λ_0 will correspond to reconstruction distances which are off focus by $\pm sg$. The spectral resolution limit d_s is estimated from the intensity distribution of a spherical wave on a plane at a distance of $z = sg$ from a point source, Eq. (6),

$$I = I_0 z \left(z^2 + d_s^{\,2}\right)^{-1.5} \propto \left(1 + \left(\frac{d_s}{sg}\right)^2\right)^{-1.5}. \tag{6}$$

#209610 - $15.00 USD Received 7 Apr 2014; revised 23 May 2014; accepted 18 Jun 2014; published 23 Jun 2014
(C) 2014 OSA

As a measure for resolution we take the full width at half maximum of the intensity, which yields $d_s = 1.5\,sg$.

4. Results

4.1 Amplitude object

To determine the spatial resolution of the THz holography set-up the diffraction pattern of a Siemens star with an inner diameter of 4 mm is considered. In Fig. 3 the corresponding numerical mask and the numerically reconstructed intensity and phase maps are presented. The experimental results are given in Fig. 4. The Siemens star has been fabricated from a metal sheet of 0.1 mm thickness using laser ablation, Fig. 4 (left), together with the reconstructed intensity (center) and phase map (right).

The lateral resolution after object reconstruction is estimated from the Modulation Transfer Function (MTF) around concentric circles with decreasing diameter intersecting the spokes of the Siemens star [27]. The circumferential modulation of the reconstructed intensity of the object, averaged over the nine spokes, is shown in Fig. 5 (left) for several circle diameters from 3.0 to 0.7 mm around the center of the Siemens star. The 10% modulation level can be defined as the resolution limit and is found at 3.5 LP/mm, corresponding to a resolution of 280 µm. For simulations using a polychromatic and a monochromatic source the 10% modulation level is at around 5.8 LP/mm and 6.4 LP/mm, respectively, see Fig. 5 (right) corresponding to lateral resolutions of 170 µm and 155 µm.

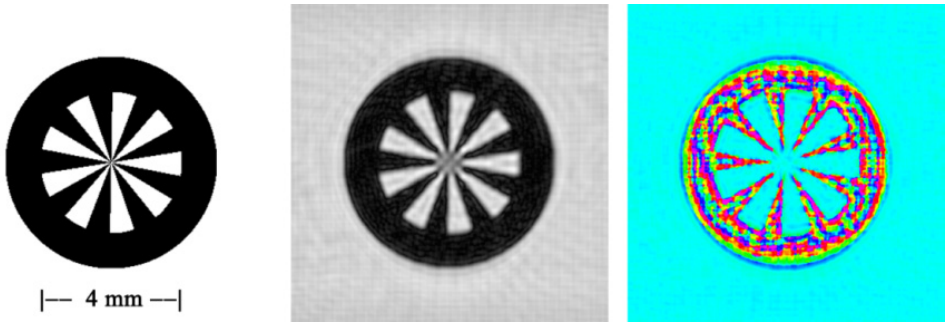

Fig. 3. Simulation: Object mask (left), reconstructed intensity (center) and phase map (right) obtained from the simulated diffraction pattern of the object mask.

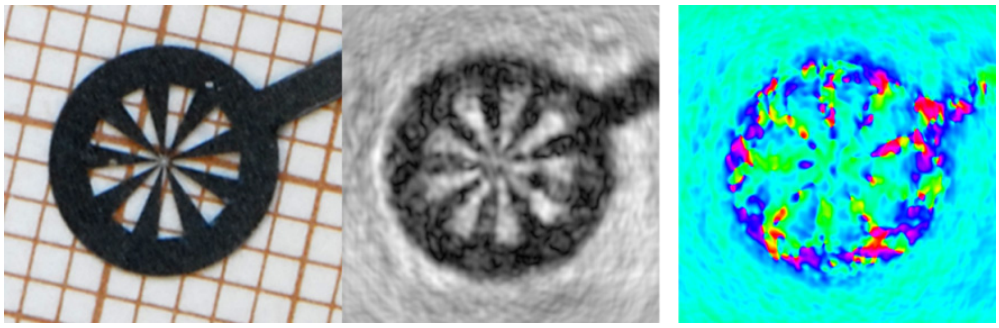

Fig. 4. Experiment: Object (left), reconstructed intensity (center) and phase map (right) obtained from the measured diffraction pattern of the object.

#209610 - $15.00 USD Received 7 Apr 2014; revised 23 May 2014; accepted 18 Jun 2014; published 23 Jun 2014
(C) 2014 OSA

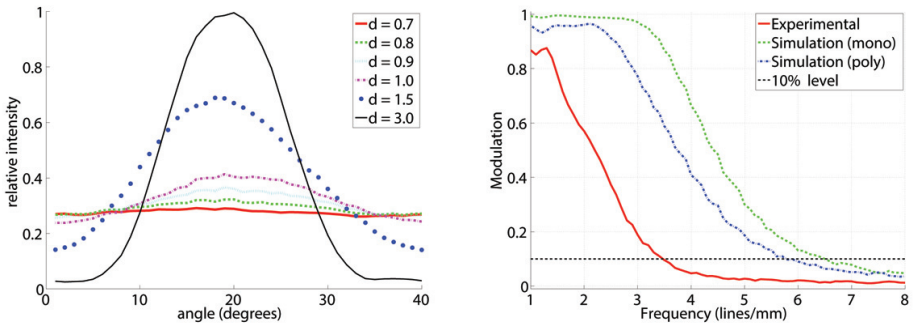

Fig. 5. Estimation of lateral resolution from circumferential MTF. Average modulation of the signal around circles with diameter d = 3.0 to 0.7 mm (left) from the experimental reconstructed intensity map of Fig. 4. Comparison of the experimental MTF to the simulated ones for mono- and polychromatic THz radiation (right).

For an object distance of 18 mm the theoretical resolution due to the NA alone, Eq. (4), is d_W = 150 µm. The resolution limitation expected from the spectral separation of two emission lines of our QCL yields d_s = 340 µm for s = 0.0125 and g = 18 mm, Eq. (6). This rather conservative estimate is a factor of two larger than the simulated values for the polychromatic source. This can be explained by the limited NA of the reconstruction.

4.2 Phase object

To determine the phase resolution of the THz holography set-up the diffraction pattern of a structured polypropylene plate with rings of different depths is considered. In Fig. 6 the numerically reconstructed intensity and phase maps are presented, while Fig. 7 shows the object image and experimental results.

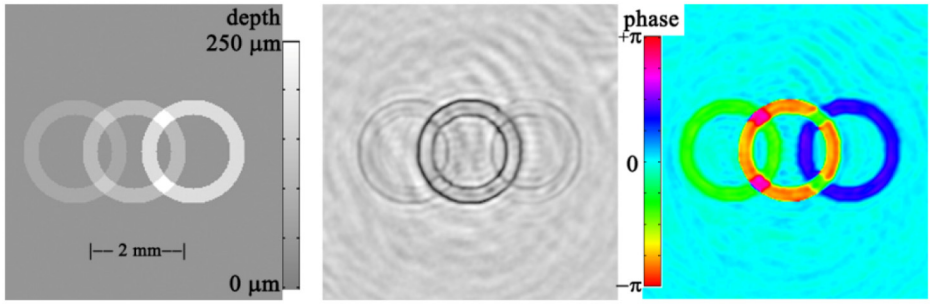

Fig. 6. Simulation: Depth image (left), reconstructed intensity (center) and phase map (right) obtained from the simulated diffraction pattern of the object using a polychromatic source.

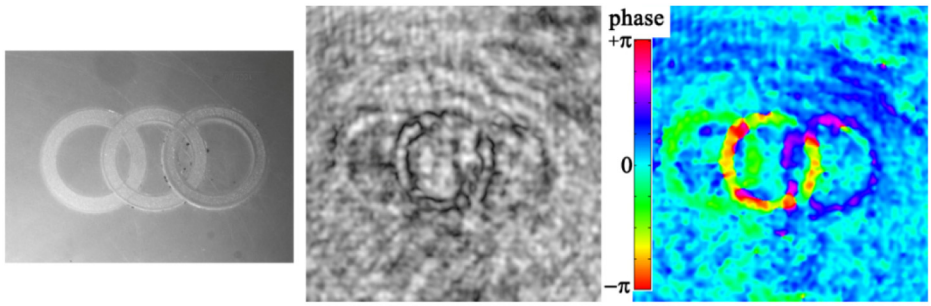

Fig. 7. Experiment: Optical image of test structure (left), reconstructed intensity (center) and phase map (right) obtained from the measured diffraction pattern of the object.

#209610 - $15.00 USD Received 7 Apr 2014; revised 23 May 2014; accepted 18 Jun 2014; published 23 Jun 2014
(C) 2014 OSA

The phase difference values are estimated from averaging the phases in the center of the rings, in the crossings of the rings and on a background line. Table 1 compares these values with the predicted phase difference values obtained from optical depth measurements and the refractive index of polypropylene n (3 THz) = 1.51. The estimated depth of the ring crossings has a higher uncertainty because the lateral resolution of them is rather low. From the standard deviation of the THz measurements we can estimate a phase difference resolution of 0.5 rad, corresponding to a 16 µm thickness variation in polypropylene.

Table 1. Phase values (mean and standard deviation) from THz measurements, Fig. 7, and expected values from optical depth measurements. Numbers in brackets show the estimated standard deviation in units of the least significant digit.

	THz Measurement	Optical prediction	Depth
Left ring	1.0 (5) rad	1.2 (1) rad	37 (3) µm
Middle ring	2.2 (5) rad	2.4 (1) rad	77 (3) µm
Right ring	5.1 (5) rad	5.0 (1) rad	157 (3)µm
Crossings left/middle ring	3.9 (8) rad	3.7 (1) rad	117 (3) µm
Crossings middle/right ring	6.3 (8) rad	7.4 (1) rad	234 (3) µm

Note that for the mapping of phase differences to depth prior knowledge of the approximate object profile and index of refraction are needed to resolve phase ambiguity. Measurements using dual wavelengths [28] could resolve phase ambiguity.

An estimation of the achievable phase resolution for our measurement geometry was again made with simulations for a polychromatic and a monochromatic source, yielding resolutions of 0.2*0* rad and 0.12 rad, corresponding to *a* thickness *of* 6 µm and 4 µm in PP, respectively. These resolution values compare favorably to pulsed THz systems, where thickness is measured by optical delay lines and typically achieve a resolution of 10 µm [29, 30] while high-resolution time-of-flight methods achieve micron resolution [4], both at the expense of scanning.

5. Conclusions

In THz holography, lateral resolution is limited by three factors: numerical aperture, sensor pitch, and spectral spread of the source. Simulations of polychromatic sources show that resolution scales with distance g and the spread of the wavelength distribution. For our configuration the resolution loss due to polychromatism is of the same order as the intrinsic resolution from the restricted aperture. Both could be improved using shorter distances to the detector. However the off-axis geometry limits the distance, since the reference beam must not interfere with the sample. This is alleviated in our set-up because the detector pixel size is only one fourth of the wavelength, which allows much larger angles for the off-axis reference beam to be used.

Phase information is essential for a faithful reconstruction of the object from its diffraction pattern using THz holography. For a phase object the reconstructed intensity image is of minor importance, as intensity contrast is low. But it can provide additional evidence for the correct reconstruction distance, as the barely visible structure gets sharp contours only at that distance. The determination of a phase map with an area detector obviates the need for scanning.

Acknowledgments

We thank Prof. Jérôme Faist, Quantum Optoelectronics group, ETH Zurich, for providing us with a THz QCL chip, and Rolf Broennimann, Empa, for preparing the targets used in this work by laser ablation.